J. Chem. Sci. (2024) 136:81
https://doi.org/10.1007/s12039-024-02322-1

REGULAR ARTICLE

Microfluidic synthesis of calcium tungstate $CaWO_4$

E A MUKHANOVA*, P D KUZNETSOVA, P V MEDVEDEV,
C Y CÁRDENAS RODRIGUEZ, E R KOLOMENSKAYA, A N BULGAKOV,
S V CHAPEK, O E POLOZHENTSEV and A V SOLDATOV
Smart Materials Research Institute, Southern Federal University, Sladkova 178/24, 344090 Rostov-on-Don, Russia
*Corresponding Author. E-mail: kand@sfedu.ru

MS received 4 June 2024; revised 21 August 2024; accepted 24 September 2024

Abstract. Nowadays, microfluidic synthesis has many advantages over bulk synthesis. By controlling the flow into the microfluidic chip, we can synthesize nanoparticles with defined and precise characteristics. A continuous microfluidics synthesis of $CaWO_4$ was conducted to obtain nanoparticles with a Scheelite structure approximately 10 nm in diameter. The $CaWO_4$ nanoparticles were characterized using elemental composition, chemical structure, particle size distribution, and morphology. Calcium tungstate and its derivatives are well known for their optical properties and have great potential for medical applications. The small diameter of nanoparticles allows the synthesis of composites on their basic for theranostics in cancer treatment. Our work indicates the potential opportunity of a continuous microfluidics technique for the rapid fabrication of Scheelite-type tungstate.

Keywords. Microfluidic synthesis; Scheelite; calcium tungstate.

1. Introduction

$CaWO_4$ with a Scheelite structure has attracted a lot of attention from researchers because of its luminescent properties.[1–5] This material and its derivatives can be used in photocatalysis,[6–9] as hosts for lanthanide-activated lasers,[10–13] and as a luminophore.[14–18] It is also important as a scintillation material for detecting X-rays and gamma rays for medical purposes.[19–23] The composition, size, and morphology of the sample control all these properties. These characteristics can be controlled by synthesis.

The literature has described many methods to synthesize tungstate with a scheelite structure, such as solid-state synthesis,[14,24,25] co-precipitation method,[26–28] sol-gel synthesis,[29] microwave synthesis,[30–33] hydrothermal synthesis,[34] and sonochemical synthesis.[35] The feature of all these methods is that they are carried out in a volumetric reaction medium and flow for a long time. One of the fastest processes is microwave synthesis, which takes 10 min.[30] Microfluidic synthesis can make the process faster by using a few reagents in a microfluidic chip.[36–38] The advantage of microfluidic synthesis is also the possibility of their implementation under the control of artificial intelligence with the ability to control in situ reaction products and change conditions to obtain a material with specified parameters.[39,40]

The microfluidic synthesis of zinc tungstate has been described in the literature,[41] but with subsequent treatment under hydrothermal conditions. In our work, we studied the possibility of exclusively obtaining calcium tungstate in microfluidic synthesis without additional processing and investigated its morphology.

2. Experimental

The starting materials for the synthesis were sodium tungstate ($Na_2WO_4{\cdot}2H_2O$), calcium chloride ($CaCl_2 \cdot 2H_2O$) and trisodium citrate. All reagents were obtained from Sigma-Aldrich, were of analytical quality, and were used without further purification. As the first step, we prepared two solutions: 0.3 M of Na_2WO_4 aqueous solution and 0.3 M of $CaCl_2$ aqueous solution (by adding trisodium citrate solution as a complex agent). Each solution was mixed separately on a magnetic stirrer until a clear solution was obtained.

The $CaWO_4$ suspension was obtained under microfluidic conditions using a precision dosing

Published online: 11 November 2024

system. It consists of a series of syringe pumps and taps connected by a system of perfluoroalkoxide (PFA) tubes (see Figure 1). The crane has three ports for connecting tubes and can change the direction of flow from C–NC to C–NO (C – common port, NC – normally closed port, NO – normally open port). At the time of loading the reagents, port NO is closed, and the required reagent is taken from port NC, which, under low pressure, flows into the syringe through port C. After the download is completed, the NC port is blocked, and NO is opened. Thus, the syringe pumps can replenish themselves without the operator's attention to ensure long-term synthesis.

During the synthesis, aqueous solutions of Na_2WO_4 and $CaCl_2$ at a concentration of 0.3 M were used. They were filled into syringes, after which they were pumped to the mixing site. To ensure constant mixing, a 10-m tube was connected after the Y-connector, along which the Na_2WO_4 solution passed at a speed of 0.3 ml/min and the $CaCl_2$ solution passed at a speed of 1.2 ml/min. The resulting suspension was collected in a separate container for post-processing (centrifugation, washing, drying).

The X-ray diffraction (XRD) of the synthesized nanoparticles was measured by the D2 PHASER using Cu Kα radiation (λ = 1.5406 Å) at 30 kV and 10 mA. For the measurements, we used a low-background cuvette and the following conditions: 2θ range from 10° to 60°, step size –0.01°.

The shape and size of the synthesized nanoparticles were investigated using a Tecnai G2 Spirit TWIN microscope.

Qualitative and quantitative elemental analysis of the synthesized nanoparticles was performed using an M4 Tornado X-ray fluorescence spectrometer. The data were collected at 20–25 points on each sample surface for 10 s.

Measurements of IR spectra were carried out on a Bruker Vertex 70 spectrometer in the ATR geometry (attenuated total reflectance) using a DTGS detector and a Bruker Platinum ATR prefix. The spectra were measured in the range from 4000 to 30 cm^{-1} with a resolution of 1 cm^{-1} and 64 scans. The reference sample was air.

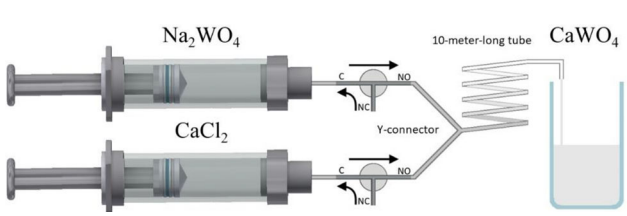

Figure 1. Illustration of the continuous synthesis of $CaWO_4$ nanoparticles.

3. Results and discussion

The results of the XRD analysis (Figure 2) show that the sample obtained in the microfluidic synthesis is single-phase with a scheelite-type structure (JCPDS 41-1431).

To obtain information about particle size and size distribution from the diffraction pattern we use the FW1/5M−FW4/5M method.[42] In this method, we can calculate the average grain size ⟨R⟩, and also draw a grain size distribution (GSD) curve that is much more informative than a single medium ⟨R⟩ parameter. Direct calculation of the average particle size and dispersion was performed using the formulas from the work.[42] The calculated average particle size and size dispersion are presented in Table 1.

The actual elemental composition percentage and the molar ratio of Ca^{2+} and W^{6+} in each sample were calculated and were obtained n(Ca) : n(W) = 0.91 : 1.00. The derivation of calcium-ion content from stoichiometry may be related to the construction of microfluidic systems and the synthesis conditions.[43,44]

The purity of the final products was monitored by FT-IR spectroscopy (Figure 3). The WO_4^{2-} tetrahedrons in Scheelite-structured tungstate show absorption bands in the region of 400–1000 cm^{-1}. The weak bands at 3425.2 and 1615.3 cm^{-1} are assigned to the O–H stretching vibration and the H–O–H bending vibration, respectively. These two bands are the characteristic vibrations of water that correspond to the physical absorption on the sample surface. A strong absorption band at 822.4 cm^{-1} is related to O–W–O stretches of the WO_4^{2-} tetrahedron, and that at

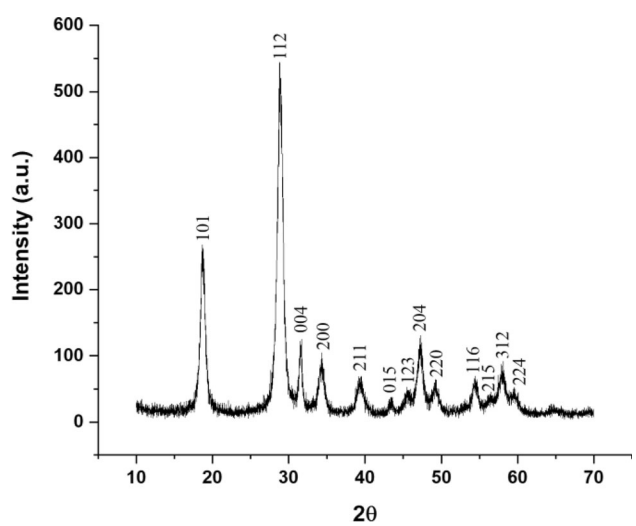

Figure 2. X-ray diffraction pattern of $CaWO_4$ nanoparticles

Table 1. The results of processing diffraction pattern by the FW1/5M−FW4/5M method for $CaWO_4$.

Sample	Size average, ⟨R⟩ (nm)	Size dispersion, σ (nm)	Relative width, $\sigma/\langle R\rangle$
$CaWO_4$ by microfluidic synthesis	13.4	4.4	0.33

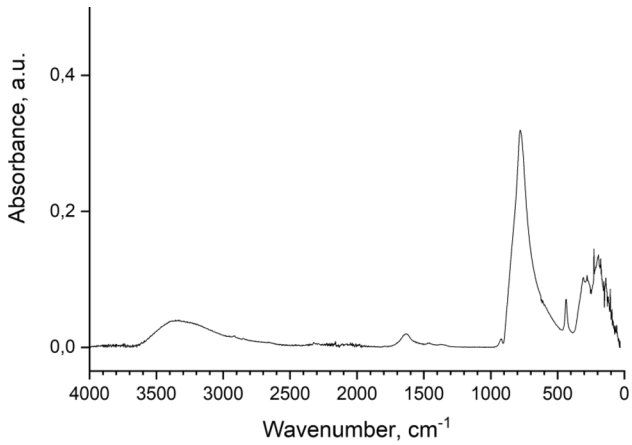

Figure 3. FTIR spectra of $CaWO_4$ nanoparticles.

438.7 cm^{-1} is attributed to the stretching vibration of W–O.[45]

The shape and size of the nanoparticles were studied by transmission electron microscopy. As seen from the TEM images and analysis in Figure 4, most of the $CaWO_4$ samples are spherical particles. The size distribution of nanoparticles was estimated using the ImageJ program and TEM images.[46,47] The average size of the nanoparticles is approximately 9 nm, but they tend to agglomerate. This size is much smaller than the particles obtained even in the ultrasonic synthesis method, the size of which is approximately 20 nm.[48]

The sizes of the synthesized samples are appropriate for further coating with SiO_2 because of their small size. Such nanoparticles overcome biological barriers.[49] Small capillaries have a diameter of approximately 3 μm, and nanoparticles with a size of less than 200 nm can be freely transported through the circulatory system to a certain place and carry pharmaceutically active substances.

Microfluidic synthesis differs in that the mixing of reagents and the reaction itself occurs in a flow of open channels with a special pattern.[37,50] These flows are laminar, directional, and highly symmetric compared with flask synthesis.[36] The channel size and location reduce the distance required for the diffusion of the interacting particles and increase the reaction rate. The microfluidic chip also allows the control of the stages of nucleation and growth of nanoparticles, depending on the shape of channels in the chip, mixing speed, and so on.[38] This leads to the possibility of accurate repeating of particle sizes and their morphology during the synthesis.

Thus, synthesis using microfluidic technologies makes it possible to obtain tungstate with a size of less than 10 nm, with a narrow size distribution of spherical shape. We controlled the particle's size by both the channel size and the mixing rate of reagents into the microfluidic chip. The next part of this work is to study the dependence of particle size and optical properties on the ratio of flow rates in the synthesis.

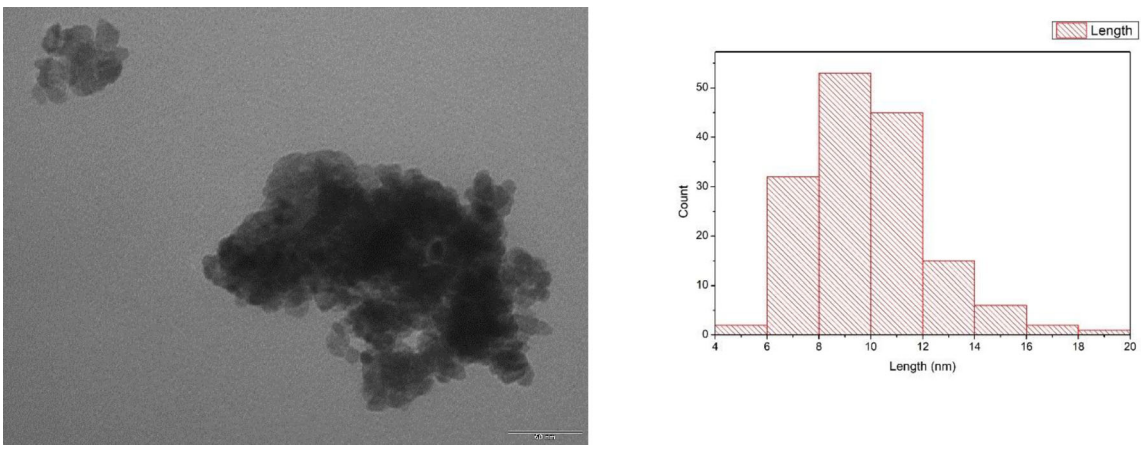

Figure 4. *Left*: TEM images of the $CaWO_4$ nanoparticles; *Right*: particle size distribution of $CaWO_4$.

4. Conclusion

In this work, we obtained calcium tungstate with a scheelite structure without additional temperature treatment, which is widely used in various fields of medicine, energy, and materials science, using rapid microfluidic synthesis. The proposed method using an automatic control system with AI allows not only to obtain specified sizes of materials in the range of 6–8 nm with a narrow size distribution but also to control synthesis. Currently, work is underway to create a model for controlling the synthesis and parameters of the obtained materials based on operando analysis.

Further work is needed to study the influence of channel sizes (radius and length), their material, and shape on the morphology of the obtained materials, the reaction yield, and the tendency of the system to clog. The improvement of microfluidic systems and their combination with artificial intelligence will allow not only the reproducible synthesis of a large family of complex oxides but also point-by-point control of their properties for specific applied research.

Acknowledgment

This research was funded by the Russian Science Foundation (Grant No. 19-15-00305-P).

References

1. Muller O and Roy R 1974 *The major ternary structural families* (Springer-Verlag: New York)
2. Blasse G and Grabmaier B C 1994 *Luminescent Materials* (Springer: Berlin, Heidelberg)
3. Xiong F B, Lin H F, Wand L J, Shen H X, Wang Y P and Zhu W Z 2015 Luminescent properties of red-light-emitting phosphors $CaWO_4$:Eu^{3+}, Li^+ for near UV LED *Bull. Mater. Sci.* **38** 1867
4. Du C, Lang F, Su Y and Liu Z 2013 Low temperature nanocasting synthesis of lanthanide ions (Ln = Tb, Eu, Dy) doped $CaWO_4$ mesoporous structure with efficiently luminescent properties *J. Colloid Interface Sci.* **394** 94
5. Zorenko Yu, Gorbenko V, Zorenko T, Savchyn V and Voloshinovskii A 2014 Luminescent and scintillation properties of $CaWO_4$ and $CaWO_4$:Bi single crystalline films, *in: International Conference on Oxide Materials for Electronic Engineering – Fabrication, Properties and Applications (OMEE-2014)*. IEEE. p. 253
6. Farsi H and Barzgari Z 2014 Synthesis, characterization and electrochemical studies of nanostructured $CaWO_4$ as platinum support for oxygen reduction reaction *Mater. Res. Bull.* **59** 261
7. Alencar L D da S, Lima N A, Mesquita A, Probst L F D, Batalha D C, Rosmaninho M G, Fajardo H V, Balzer R and Bernardi M I B 2018 Effect of different synthesis methods on the textural properties of calcium tungstate ($CaWO_4$) and its catalytic properties in the toluene oxidation *Materials Res.* **21**
8. Georgieva R, Gancheva M, Ivanov G, Shipochka M, Markov P, Nihtianova D, Iordanova R and Naydenov A 2021 Synthesis, characterization and activity of Pd/$CaWO_4$ catalyst in the complete oxidation of C1–C6 alkanes and toluene *Reaction Kinetics, Mechanisms and Catalysis* **132** 811
9. Gao H, Wang S, Wang Y, Yang H, Wang F, Tang S, Yi Z and Li D 2022 $CaMoO_4$/$CaWO_4$ heterojunction micro/nanocomposites with interface defects for enhanced photocatalytic activity *Colloids Surf. A Physicochem. Eng. Asp.* **642** 128642
10. Wang X, Wang Y, Bu Y, Yan X, Wang J, Cai P, Vu T, and Seo H J 2017 Influence of doping and excitation powers on optical thermometry in Yb^{3+}–Er^{3+} doped $CaWO_4$ *Sci. Rep.* **7** 43383
11. Flournoy P A and Brixner L H 1965 Laser characteristics of niobium compensated $CaMoO_4$ and $SrMoO_4$ *J. Electrochem. Soc.* **112** 779
12. Xu W, Cui Y, Hu Y, Zheng L, Zhang Z and Cao W 2017 Optical temperature sensing in Er^{3+}–Yb^{3+} co-doped $CaWO_4$ and the laser-induced heating effect on the luminescence intensity saturation *J. Alloys Compd.* **726** 547
13. Li L, Qin F, Zhou Y, Miao J and Zhang Z 2019 Experimental insight into the thermal quenching of the Tb^{3+} ion's green photoluminescence in $CaWO^4$ host *Jpn. J. Appl. Phys.* **58** 110909
14. Tsuchiya Y, Hagiwara M and Fujihara S 2018 Fluorochromic properties of undoped and Ln^{3+}-doped $CaWO_4$ phosphor particles *ECS J. Solid State Sci. Technol.* **7** R50
15. Carcia P F, Reilly M, Torardi C C, Crawford M K, Miao C R and Jones B D 1997 Vapor-deposited $CaWO_4$ phosphor *J. Mater. Res.* **12** 1385
16. Cheng X, Yuan C, Su L, Wang Y and Zhu X 2014 Effects of pressure on the emission of $CaWO_4$:Eu^{3+} phosphor *Opt. Mater. (Amst.)* **37** 214
17. Zhou X, Wang R, Xiang G, Jiang S, Li L, Luo X, Pang Y and Tian Y. 2017 Multi-parametric thermal sensing based on NIR emission of Ho(III)-doped $CaWO_4$ phosphors *Opt. Mater. (Amst.)* **66** 12
18. Bakovets V V, Zolotova E S, Antonova O V, Korol'kov I V and Yushina I V 2016 Possibility of adjusting photoluminescence spectra of Ca scheelites ($CaMoO_4$: Eu^{3+} and $CaWO_4$: Eu^{3+}) to the emission spectrum of incandescent lamps *Technical Phys.* **61** 1064
19. Martini N, Koukou V, Fountos G, Valais I, Kandarakis I, Michail C, Bakas A, Lavdas E, Ninos K, Oikonomou G, Gogou L and Panayiotakis G 2019 Imaging performance of a $CaWO_4$/CMOS sensor *Frattura ed Integrità Strutturale* **13** 471
20. Koukou V, Martini N, Valais I, Bakas A, Kalyvas N, Lavdas E, Fountos G, Kandarakis I and Michail C. 2017 Resolution properties of a calcium tungstate ($CaWO_4$) screen coupled to a CMOS imaging detector *J. Phys. Conf. Ser.* **931** 012027
21. Kim J-N, Shin J-W, Oh K-M, Lee Y-K, Park S-K, Park J-K and Nam S-H 2013 Optimization of nano-phosphor synthesis by including sensitizer doping for medical X-Ray imaging *J. Nanosci. Nanotechnol.* **13** 3455

22. Mattner A, Zimmermann L, Lienenklaus S, Weiss S and Wickleder C 2020 Tailoring long-lasting luminescence of red-emitting $CaWO_4$:Eu^{3+}, Sm^{3+} nanoparticles with enhanced crystallinity for improved bio-imaging *Ceram. Int.* **46** 26295
23. Akman F, Kaçal M R, Almousa N, Sayyed M I and Polat H 2020 Gamma-ray attenuation parameters for polymer composites reinforced with $BaTiO_3$ and $CaWO_4$ compounds *Prog. Nuclear Energy* **121** 103257
24. Flor G, Massarotti V and Riccardi R 1977 On the mechanism of $CaWO_4$ formation in the solid state from CaO and WO_3 *Z. Natur. A* **32** 160
25. Wu H, Niu P, Pei R, Zheng Y, Jin W, Li X-M and Jiang R 2021 Tb^{3+} and Sm^{3+} co-doped $CaWO_4$ white light phosphors for plant lamp synthesized via solid state method: Phase, photoluminescence and electronic structure *J. Lumin.* **236** 118146
26. Yang Y, Wang X and Liu B 2014 Synthesis of $CaWO_4$ and $CaWO_4$:Eu microspheres by precipitation *NANO* **9**
27. Thongtem T, Kungwankunakorn S, Kuntalue B, Phuruangrat A and Thongtem S 2010 Luminescence and absorbance of highly crystalline $CaMoO_4$, $SrMoO_4$, $CaWO_4$ and $SrWO_4$ nanoparticles synthesized by co-precipitation method at room temperature *J. Alloys Compd.* **506** 475
28. Jung J, Kim J, Shim Y-S, Hwang D and Son CS 2020 Structure and photoluminescence properties of rare-earth (Dy^{3+}, Tb^{3+}, Sm^{3+})-doped $BaWO_4$ phosphors synthesized via Co-precipitation for anti-counterfeiting *Materials* **13** 4165
29. Mickens M, Assefa Z and Kumar D 2012 Tunable white light-emission of a $CaW_{1-x}Mo_xO_4$:Tm^{3+}, Tb^{3+}, Eu^{3+} phosphor prepared by a Pechini sol–gel method *J. Solgel Sci. Technol.* **63** 153
30. Li Q, Shen Y and Li T 2013 Fast microwave-assisted synthesis and photoluminescence of $CaWO_4$ nanocrystals. *J. Chem.* 952954
31. Dhilip Kumar R and Karuppuchamy S 2014 Microwave-assisted synthesis of copper tungstate nanopowder for supercapacitor applications *Ceram. Int.* **40** 12397
32. Zheng Y, Lin J and Wang Q 2012 Emissions and photocatalytic selectivity of $SrWO_4$:Ln^{3+} (Eu^{3+}, Tb^{3+}, Sm^{3+} and Dy^{3+}) prepared by a supersonic microwave co-assistance method *Photochemical and Photobiological Sci.* **11** 1567
33. Liu X, Lv L, Huang S, Su Y and Wang X 2014 Microwave-assisted synthesis and luminescence properties of $Cd_{1-x}Eu_xMoO_4$ red phosphor *J. Nanosci. Nanotechnol.* **14** 3618
34. Wang X Z 2014 Hydrothermal synthesis and luminescence of MWO_4:Tb^{3+} (M = Ca, Sr, Ba) microsphere phosphors *J. Materials Sci.: Materials in Electronics* **25** 3271
35. Janbua J, Mayamae J, Wirunchit S, Baitahe R and Vittayakorn N 2015 Directed synthesis, growth process and optical properties of monodispersed $CaWO_4$ microspheres via a sonochemical route *RSC Adv.* **5** 19893
36. Abou-Hassan A, Sandre O and Cabuil V 2010 Microfluidics in inorganic chemistry *Angew. Chem. International Edition* **49** 6268
37. Jahn A, Reiner J E, Vreeland W N, DeVoe D L, Locascio L E and Gaitan M 2008 Preparation of nanoparticles by continuous-flow microfluidics *J. Nanoparticle Res.* **10** 925
38. Rial R, Tahoces P G, Hassan N, Cordero M L, Liu Z and Ruso J M 2019 Noble microfluidic system for bioceramic nanoparticles engineering *Materials Sci. Eng. C* **102** 221
39. Liu L, Bi M, Wang Y, Liu J, Jiang X, Xu Z and Zhang X 2021 Artificial intelligence-powered microfluidics for nanomedicine and materials synthesis *Nanoscale* **13** 19352
40. Seo H and Lee H 2021 Recent developments in microfluidic synthesis of artificial cell-like polymersomes and liposomes for functional bioreactors *Biomicrofluidics* **15** 021301
41. Chen Z, Song Q, Ni L, Jiang J and Yu Y 2021 Microfluidic synthesis of $ZnWO_4$ nanoparticles and its performance in DMSO-containing wastewater treatment *J. Environ. Chem. Eng.* **9** 106528
42. Pielaszek R 2004 FW1/5/4/5M method for determination of the grain size distribution from powder diffraction line profile *J. Alloys Compd.* **382** 128
43. Poonoosamy J, Mahrous M, Curti E, Bosbach D, Deissmann G, Churakov S V, Geisler T, and Prasianakis N 2021 A lab-on-a-chip approach integrating *in-situ* characterization and reactive transport modelling diagnostics to unravel (Ba, Sr) SO_4 oscillatory zoning *Scientific Rep.* **11** 23678
44. Fuest M, Rangharajan K K, Boone C, Conlisk A T and Prakash S 2017 Cation-dependent surface charge regulation in gated nanofluidic devices *Anal. Chem.* **89** 1593
45. Dabre K and Dhoble S 2013 Thermoluminescence glow curve analysis of Eu^{3+} activated $CaWO_4$ phosphor *Adv. Mater. Lett.* **4** 921
46. Schneider C A, Rasband W S and Eliceiri K W 2012 NIH image to imageJ: 25 years of image analysis *Nat. Methods* **9** 671
47. Schindelin J, Arganda-Carreras I, Frise E, Kaynig V, Longair M, Pietzsch T, Preibisch S, Rueden C, Saalfeld S, Schmid B, Tinevez J-Y, White D J, Hartenstein V, Eliceiri K, Tomancak P and Cardona A 2012 Fiji: an open-source platform for biological-image analysis *Nat. Methods* **9** 676
48. Mukhanova E A, Pankin I A, Polozhentsev O E, Kuznetsova P D, Polyakov V A and Soldatov A V 2022 Influence of the methods of synthesis and grain size distribution on XEOL spectra of $CaWO_4$:xTb^{3+} *Inorg. Chem. Commun.* **140** 109407
49. Blanco E, Shen H and Ferrari M 2015 Principles of nanoparticle design for overcoming biological barriers to drug delivery *Nat. Biotechnol.* **33** 941
50. Lai J J, Nelson K E, Nash M A, Hoffman A S, Yager P and Stayton P S 2009 Dynamic bioprocessing and microfluidic transport control with smart magnetic nanoparticles in laminar-flow devices *Lab Chip.* **9** 1997